Ultrastructure of Human Erythrocyte GLUT1†

C. Graybill,‡ A. N. van Hoek,§ D. Desai,‡ A. M. Carruthers,‡ and A. Carruthers*,‡

Department of Biochemistry and Molecular Pharmacology, University of Massachusetts Medical School, 364 Plantation Street, Worcester, Massachusetts 01606, and Renal Unit and Department of Pathology, Massachusetts General Hospital and Harvard Medical School, Boston, Massachusetts 02114

Received February 27, 2006; Revised Manuscript Received May 4, 2006

ABSTRACT: This study was undertaken to examine GLUT1 quaternary structure. Independent but complementary methodologies were used to investigate the influence of membrane-solubilizing detergents on GLUT1/lipid/detergent micelle hydrodynamic radii. Hydrodynamic size analysis and electron microscopy of GLUT1/lipid/detergent micelles and freeze-fracture electron microscopy of GLUT1 proteoliposomes support the hypothesis that the glucose transporter is a multimeric (probably tetrameric) complex of GLUT1 proteins. GLUT1 forms a multimeric complex in octyl glucoside that dissociates upon addition of reductant. Some detergents (e.g., CHAPS and dodecyl maltoside) promote the dissociation of GLUT1 oligomers into smaller aggregation states (dimers or monomers). These complexes do not reassemble as larger oligomers when dissociating detergents are subsequently replaced with nondissociating detergents such as octyl glucoside or cholic acid. When dissociating detergents are replaced with lipids, the resulting proteoliposomes catalyze protein-mediated sugar transport, and the subsequent addition of solubilizing, nondissociating detergents generates higher (tetrameric) GLUT1 aggregation states. These findings suggest that some detergents stabilize while others destabilize GLUT1 quaternary structure. GLUT1 does not appear to exchange rapidly between protein/lipid/detergent micelles but is able to self-associate in the plane of the lipid bilayer.

A diverse group of polytopic integral membrane proteins called transporters catalyzes solute transport across cell membranes. These transporters form two major subgroups: the channels and the carriers (*1*). Several channels have been successfully crystallized and subjected to detailed structural analysis by X-ray diffraction. Relatively few carriers have been amenable to structural analysis.

Understanding the three-dimensional structure of the transporters is important for several reasons. (1) With relatively few exceptions, the helix packing of transporters has not been determined by available computational algorithms (*2, 3*). (2) Polytopic integral membrane proteins are largely refractory to biochemical approaches to high-resolution characterization of substrate and ligand binding sites (e.g., compare ref *4* with refs *5* and *6*). Thus, a three-dimensional structure would greatly facilitate identification of putative substrate binding domains and transport pathways for verification or refutation by mutagenesis. (3) Biochemical and molecular biological analyses of transporters of previously unknown structure may now be interpreted with the context of a specific three-dimensional structure. These advantages together with the ability to target specific sites for labeling with environmentally sensitive probes will ultimately lead to a more comprehensive understanding of the molecular mechanisms of channel- and carrier-mediated transport.

Three general challenges remain in crystallization studies of membrane transporters: (1) obtaining high-quality crystals of membrane transporters, (2) obtaining crystals of each transporter conformation of the transport cycle, and (3) resolving whether the quaternary structure of the transporter in the crystal corresponds to that of the transporter in the cell membrane. For challenge 2, for example, with some carriers, there are at least four, and as many as 12, intermediate kinetic states that have been identified biochemically or via steady-state transport assays (*7*). Since the challenge is to understand how transporters transition from one conformational state to the next, it is important that each of these states be resolved.

Glucose transport across cell membranes is carrier-mediated. Two classes of glucose transport are observed. Active transport is effected by the SGLT family of integral membrane proteins in which the net accumulation or uptake of glucose is coupled to and driven by the net flow of a cation, normally sodium, down its electrochemical gradient into the cell (*8*). Passive, carrier-mediated glucose transport is catalyzed by the GLUT family of integral membrane proteins. These carriers mediate the rapid bidirectional flow of sugars into and out of the cell (*9*). However, the net direction of passive transport is always from high to low sugar concentration. These transporters are typically faster than the active transporters (*1*). Absorptive and reabsorptive cells of the small intestine and proximal tubule express the SGLT family of proteins at the luminal face of the cell and the GLUT transporters at the serosal or blood side of the cell. In this way, cells can catalyze the net flow of sugars against a concentration gradient into the cell

† This work was supported by NIH Grants DK 44888 and DK 36081.

* To whom correspondence should be addressed. Phone: (508) 856-5570. Fax: (508) 856-6464. E-mail: anthony.carruthers@umassmed.edu.

‡ University of Massachusetts Medical School.

§ Massachusetts General Hospital and Harvard Medical School.

10.1021/bi060398x CCC: $33.50
Published on Web 06/10/2006

and down a concentration gradient to the blood side of the cell.

The passive glucose transporter that has been most extensively studied is human red blood cell GLUT1.[1] This protein comprises almost 10% of the integral membrane proteins in erythrocytes (*10*). Although a high-resolution, crystal structure of GLUT1 is unavailable, related major facilitator superfamily (MFS) transporters LacY and GlpT of *Escherichia coli* have been crystallized and resolved to 3.5 and 3.3 Å resolution, respectively (*3*, *11*). These structures support the hypothesis that MFS carriers present a substrate-binding cavity that is alternately exposed to interstitium and cytoplasm. Salos-Burgos et al. (*12*) have used the GlpT structure as a homology template for modeling GLUT1 structure, and the resulting structure (PDB entry 1SUK) provides significant insights into GLUT1 biochemistry and function.

Being relatively uniform in shape, surface area, and volume, human red blood cells are a very useful model for kinetic analysis of carrier-mediated sugar transport. Analysis of sugar transport by human red blood cells in the presence of inhibitors suggests that the glucose transporter complex presents at least two sugar uptake sites and at least two sugar export sites at any instant (*13*, *14*). This view is reinforced by analysis of ligand binding to sugar uptake and sugar efflux sites of the glucose transporter in human red cells indicating that each transporter presents multiple sugar uptakes and sugar exit sites simultaneously in the red cell (*15*). However, each glucose transport protein, when studied in isolation, appears to function as an alternating conformer carrier protein in which the transport protein alternates between a sugar import (e2) and a sugar export (e1) state (*16*−*18*). Import and export states appear to be mutually exclusive in vitro.

This apparently contradictory behavior was resolved when we learned that the glucose transport protein exists as a GLUT1 multimer in the red cell membrane and in certain detergents (*18*). This laboratory has proposed that the glucose transporter of human red cells is a GLUT1 homotetramer in which each subunit is a functional transport pathway. At any instant, two subunits must exist in an import or e2 state while the remaining two subunits must exist in an e1 or export competent state. In this way, the transporter presents uptake and efflux sites simultaneously, but each subunit functions as a classic e1 or e2 iso-uni-ping-pong carrier (*18*, *19*).

These conclusions are based upon several assumptions: (1) The ligands cytochalasin B and maltose bind at the sugar exit and sugar import sites, respectively. (2) Chemical cross-linking of cell membrane-resident transporter produces cross-linked states that accurately reflect the quaternary structure of the protein in the cell membrane. (3) The hydrodynamic properties of cholic acid-solubilized GLUT1 and Triton X-100-solubilized GLUT1 accurately reflect the quaternary structure of the glucose transport protein in cell membranes. None of these assumptions is inviolable. Maltose is known to react with import and export sites [but not in intact cells where maltose cannot penetrate the cell (*14*)]. The use of photoreactive cross-linkers with lifetimes on the order of nano- to microseconds often avoids artifactual cross-linking of spatially separated subunits in cell membranes that may, with time, collide. There is also a growing literature indicating that the hydrodynamic properties of detergent-solubilized integral membrane proteins are strongly dependent upon the nature of the detergents used to solubilize the proteins (*1*, *13*).

This study was undertaken to investigate the hydrodynamic radius of GLUT1/lipid/detergent micelles released from GLUT1 proteoliposomes upon addition of a wide range of membrane detergents. Our findings demonstrate that the quaternary structure of GLUT1 is strongly dependent upon the solubilizing detergent, and thus, great care must be exercised in extrapolating the results of such analyses to protein structure in the cell membrane.

MATERIALS AND METHODS

Materials. All reagents were purchased from Sigma Chemical unless otherwise noted. [^{3}H]Cytochalasin B was purchased New England Nuclear. Triton X-100 and octyl β-glucoside were purchased from Calbiochem. Cholic acid, deoxycholate, CHAPS, CHAPSO, dodecyl maltoside, Tween 20, and Big CHAPS were purchased from Pierce.

Solutions. Saline consisted of 150 mM NaCl, 5 mM HEPES, and 0.2 mM EDTA (pH 7.2). Potassium medium (kaline) comprised 150 mM KCl, 5 mM HEPES, and 0.2 mM EDTA (pH 7.2). Lysis medium consisted of 10 mM HEPES and 0.2 mM EDTA (pH 7.2). Tris medium consisted of 50 mM Tris-HCl and 0.2 mM EDTA (pH 7.4). Alkaline wash medium consisted of 12.5 mM NaOH and 5 mM EDTA (pH 12.0).

Glucose Transport Protein. Human red blood cells were obtained from whole human blood by centrifugation at 14000*g* for 10 min into volumes of saline or kaline at 4 °C. The supernatant and the white buffy coat were aspirated and the cells resuspended into volumes of saline or potassium medium. The centrifugation wash cycle was repeated until the white buffy coat was no longer visible to the naked eye. The resulting red cell suspension was stored at 4 °C until further use. Red cell ghosts were prepared from freshly prepared human red cells by a series of washes in hypotonic lysis medium. One volume of packed red cells was added to at least 40 volumes of lysis medium at 4 °C. The suspension was stirred slowly for 30 min on ice and centrifuged at 20000*g* for 20 min. The supernatant was aspirated, and the cell membrane pellet was resuspended in 40 volumes of lysis medium. The centrifugation wash cycle was repeated until the cell membrane pellet was white. This normally required five to eight wash centrifugation cycles. The resulting membranes were adjusted to a concentration of 4 mg of protein/mL in lysis medium and then frozen at −80 °C until further use. Red cell integral membrane proteins were prepared from red cell ghost membranes by suspending 1 volume of ghost membranes at 4 mg/mL in 5 volumes of alkaline wash medium. The suspension was allowed to sit at 4 °C for 30 min, and then the membranes were collected

[1] Abbreviations: GLUT1, human erythrocyte glucose transport protein; 3MG, 3-*O*-methylglucose; CCB, cytochalasin B; CCD, cytochalasin D; CHAPS, 3-[(3-cholamidopropyl)dimethylammonio]-1-propanesulfonate; CHAPSO, 3-[(3-cholamidopropyl)dimethylammonio]-2-hydroxy-1-propanesulfonate; DDM, dodecyl maltoside; EDTA, ethylenediaminetetraacetic acid; HEPES, *N*-(2-hydroxyethyl)piperazine-*N*′-2-ethanesulfonic acid; OG, octyl glucoside; RBC, red blood cell; R_h, Stokes radius or hydrodynamic radius; SDS−PAGE, sodium dodecyl sulfate−polyacrylamide gel electrophoresis; SEM, standard error of the mean; Tris-HCl, tris(hydroxymethyl)aminomethane hydrochloride.

by centrifugation at 25000*g* for 20 min. The supernatant was aspirated, and the resulting membrane pellet was washed three times in Tris medium until the pH of the suspension was 7.4. The membranes were frozen at a concentration of 2 mg of protein/mL at −80 °C.

GLUT1 was purified from human red blood cell integral membrane proteins as described previously (*18*). Integral membrane proteins at 2 mg/mL in Tris-HCl medium were adjusted to 48 mM octyl glucoside by slow addition of solid octyl glucoside. Following end-over-end rotation for 30 min at 4 °C, the clarified suspension was centrifuged at 45000*g* for 1 h at 4 °C. The clear supernatant was carefully decanted and the pellet rejected. The supernatant was than applied to a DE-52 column equilibrated with Tris-HCl medium containing 25 mM sodium chloride and 34 mM octyl glucoside. Following application of the sample to the column, the column was washed with Tris medium containing 25 mM NaCl and 34 mM octyl glucoside at a flow rate of 1 mL/min. The first 200 mL of sample eluate was collected and then dialyzed over 48 h against at least three changes of 30 volumes of Tris medium lacking octyl glucoside. The flow-through fractions contain red cell lipids, glucose transport protein, and detergent. During dialysis, the fractions become opaque in appearance due to reconstitution of the glucose transport protein into lipid membranes formed from the copurified red cell lipids.

The resulting proteoliposomes were sedimented by ultracentrifugation at 20000*g* for 15 min, adjusted to a concentration of 1 mg/mL, aliquoted into 100 mg samples, and frozen at −80 °C. The purity of the sample was checked by gel electrophoresis (see below) and by analysis of binding of [^{3}H]CCB to GLUT1 proteoliposomes (see below).

Equilibrium Cytochalasin B Binding. Equilibrium binding of [^{3}H]CCB to purified GLUT1 and to red cell membranes was assessed as described previously (*20*). Briefly, 50 μL of GLUT1 proteoliposomes or red cell membranes at 2 mg/mL membrane protein was mixed with 50 μL of [^{3}H]CCB solution in Tris medium. Two 10 μL aliquots were sampled from the suspension to give total counts. The sample was permitted to equilibrate on ice for 30 min (equilibrium binding is achieved within 5 min), and then the membranes were sedimented by centrifugation at 14000*g* for 5 min at 4 °C. Two 10 μL aliquots of the clear supernatant were then sampled as a measure of the amount of free [^{3}H]CCB. [^{3}H]-CCB specific activity associated with each sample was quantitated by liquid scintillation spectroscopy. Bound radioactivity was obtained by subtracting the free disintegrations per minute from the total disintegrations per minute. Cytochalasin B binding was assessed as a function of increasing unlabeled cytochalasin B concentration. The cytochalasin B binding capacity of purified GLUT1 ranges from approximately 0.5 mol of cytochalasin B per mole of glucose transport protein for tetrameric GLUT1 to 1 mol of cytochalasin B per mole of GLUT1 protein in dimeric GLUT1.

GLUT1 Photolabeling Using [^{3}H]Cytochalasin B. Purified GLUT1 and GLUT1 proteoliposomes were photolabeled with [^{3}H]CCB as described previously (*21*). Samples were resuspended in 700 μL of 6.25 μM [^{3}H]cytochalasin B (CCB) and 10 μM cytochalasin D (with or without 100 μM phloretin in PBS at pH 7.4) and allowed to equilibrate on ice for 10 min. This suspension was placed on ice and irradiated for 4 min at 280 nm in a Rayonet photochemical reactor. Following UV irradiation, membranes were washed with PBS to remove unbound CCB and sedimented by centrifugation (100000*g* for 15 min). Proteins were resolved on 10% SDS−PAGE gels and stained for protein. Gel slices (2 mm) were extracted from stained gels and incubated overnight at 50 °C in 300 μL of 30% H_2O_2 before addition of scintillation fluid and counting.

Rotary Shadowing Transmission Electron Microscopy. Three samples were prepared for transmission electron microscopy: (i) GLUT1 proteoliposomes, (ii) GLUT1 proteoliposomes solubilized in *n*-octyl glucoside (OG), and (iii) endogenous erythrocyte lipids solubilized in OG. GLUT1 proteoliposomes contain GLUT1 reconstituted into bilayers of endogenous erythrocyte lipids. GLUT1 proteoliposomes solubilized in *n*-octyl glucoside (OG) were prepared in 80 mM OG in 50 mM Tris-HCl and sedimented (100000*g*), and the supernatant was diluted to 40 mM OG. Erythrocyte lipids were extracted from GLUT1 proteoliposomes following the procedure described by Bligh and Dyer (*22*). Dried lipids were then resuspended in 80 mM OG and sedimented (100000*g*), and the supernatant was diluted to 40 mM OG.

Samples in 50 mM Tris (with or without detergent) were first diluted 1:1 (v/v) in 600 mM ammonium acetate and 50% (v/v) glycerol (pH 7.0) and sprayed onto carbon sheets made by evaporating carbon onto freshly cleaved mica. Samples were returned to the vacuum evaporator and rotary shadowed at 6° with Pd/Au (20:80). The replicas were imaged on a Philips CM 10 transmission electron microscope using an accelerating voltage of 80 kV. Image negatives were digitized and analyzed using Image SXM (formally NIH Image), and the radius distribution was fitted to two Gaussian functions of the form

$$y = \beta_1 + \alpha_1 e^{-(R_{h1}-\mu_1)^2/\sigma_1^2} + \beta_2 + \alpha_2 e^{-(R_{h2}-\mu_2)^2/\sigma_2^2} \quad (1)$$

where y is the density, β is the number of particles in the bin equivalent to the sample maximum R_h, α is the number of particles in the bin equivalent to the sample mode R_h, R_h is particle radius in nanometers, μ is the average R_h, and σ is the sample variance (bell width). Subscripts 1 and 2 correspond to particle populations 1 and 2, respectively.

Freeze-Fracture Electron Microscopy. Freeze-fracture electron microscopy of GLUT1 proteoliposomes was performed as described in ref *23*. GLUT1 proteoliposomes were fixed for 4 h in 2% glutaraldehyde, washed twice with PBS, and cryoprotected with 30% glycerol in 0.1 mM sodium cacodylate (pH 7.5) buffer. The sample was placed on a copper specimen holder and frozen by immersion in N_2-cooled Freon 22. Frozen samples were transferred into a Cressington freeze-fracture apparatus (Cressington Scientific Instruments, Watford, U.K.). The temperature of the samples was increased to −120 °C to remove Freon 22, and the membranes were fractured after approximately 20 min under a vacuum of 10^{-7} Torr. Specimens were shadowed with platinum at a 45° angle. A 1.5 nm film was deposited in unidirectional shadowing, while a 2 nm coat was utilized for rotary shadowing. Platinum shadowing was followed by deposition of a 5 nm carbon coat perpendicular to the fracture plane. The specimen was removed from the copper support in sodium hypochlorite bleach. Replicas were cleaned by several rinses in distilled water, gathered on nickel grids,

and examined in a Philips (Mahwah, NJ) CM10 electron microscope.

Fractured membranes were photographed after the specimen tilt was minimized to reduce the overestimation of the particle density and minimize errors in the determination of particle size. Some rotary-shadowed samples were utilized for comparison, and the values that were obtained did not differ significantly from the samples that were shadowed unidirectionally. IMP diameters were measured on photographs at a magnification of 630000×. The width of the electron dense deposit was measured from unidirectionally shadowed particles at right angles to the direction of shadowing. The diameter of rotary-shadowed particles was also measured. Half of the thickness of the brightly shadowed rim surrounding the IMP was included in this size measurement. The radius distribution was fitted to one of two Gaussian functions of the form shown in eq 1 (see above).

Reconstitution of GLUT1-Mediated Sugar Transport. GLUT1 was reconstituted in large unilamellar egg phosphatidylcholine/cholesterol vesicles as described previously (*24*). Egg PC (40 mg in hexane) and cholesterol (10 mg) (80:20 molar ratio) were dissolved in hexane. The organic phase was evaporated under a stream of N_2, and remaining trace quantities of hexane were removed in vacuo for 3 h. The resulting lipid film was dissolved in Tris medium containing 5% (by weight) sodium cholate and mixed with 100 μg of GLUT1 solubilized in 50 mM sodium cholate. This mixture (4 mL) was dialyzed overnight against 6 L of detergent-free Tris medium, and the resulting suspension of small unilamellar proteoliposomes was distributed in 0.5 mL fractions in microcentrifuge tubes. Each tube was frozen in a dry ice/isopropyl alcohol mixture, thawed at room temperature, and then subjected to two additional rounds of freezing and thawing. The resulting large unilammelar proteoliposomes (mean diameter of 2.5 μm by oil immersion phase contrast) sedimented readily at 14000*g* and were used for sugar transport determinations at 24 °C. 3OMG uptake (0.05 mM) was assessed in 100 μL of proteoliposome suspension (2 μg of GLUT1) at 0, 10, 20, 30, and 60 s in Tris medium with or without 10 μM CCB [a transport inhibitor; $K_{i(app)} = 0.2$ μM]. Equilibrium uptake was assessed by incubation for 2 h at 24 °C. Uptake was arrested by addition of 1 mL of ice-cold Tris medium containing 10 μM CCB. Proteoliposomes were sedimented by centrifugation at 14000*g* for 5 min at 4 °C; the supernatant was aspirated, and the liposomes were washed again in Tris medium containing CCB. Uptake, v, was computed as

$$v = \frac{[3MG]}{t}\frac{cpm_t - cpm_0}{cpm_\infty - cpm_0}$$

where [3MG] is the 3MG concentration, t is time, and cpm_0, cpm_t, and cpm_∞ correspond to the radioactivity associated with proteoliposomes at time zero, time t, and equilibrium, respectively.

Analytical Procedures. SDS−PAGE was carried out using 10 or 15% acrylamide gels as described previously (*25*). Samples were not boiled prior to application to the gel. Protein assays were carried out using the Pierce BCA (bicinchoninic acid) assay. Linear regression and nonlinear regression analyses were carried out using Kaleidagraph (Synergy Software). Image analysis was carried out using Image SXM (http://www.liv.ac.uk/~sdb/ImageSXM/).

Determination of Hydrodynamic Radii. The particle hydrodynamic radius was determined using two methods. The first method was analytical size exclusion HPLC using a Toso Haas TSK 4000 column as described previously (*18*). The column was calibrated using hydrodynamic standards obtained from Pierce and was developed at a flow rate of 0.3 mL/min. Samples (100 μL) were injected onto the column in a variety of detergents. All solutions and all samples following preparation were filtered through 0.2 μm filters prior to application to the column. Samples emerging from the column were detected by UV absorbance at 280 nm, by differential refractive index measurements, and by light scattering at 15° and 90° using a Precision Detectors 2000 N System. This detection system further permits the computation of dn/dC for each sample as it passes through the detector and, in combination with the low and 90° angle light scattering data, allows calculation of the mass of the particle emerging from the column.

Hydrodynamic radii were also determined by dynamic light scattering by using a Precision Detectors 2000 Cool Batch System. This system detects the Brownian motion of particles in a small (100 μL) cuvette by analysis of rapid (microseconds) fluctuations in scattered light. These data are then used to compute the diffusion coefficient of the particles. All solutions were filtered through a 0.2 μm filter prior to use. Glucose transport protein, following solubilization in the appropriate detergent, was collected as the ultracentrifugation supernatant (Beckman airfuge, 200000*g*) and filtered again through a 0.2 μm filter prior to analysis in the cuvette-based system. Although the cuvette-based system does not require calibration, the accuracy of the analysis was checked by analysis of the hydrodynamic radius of a variety of standards obtained from Pierce Chemicals. Analyses of hydrodynamic radii were carried out between 10 and 35 °C using the Cool Batch built-in Peltier device. The cuvette was flushed with filtered nitrogen to prevent condensation on the face of the cuvette during measurements.

Particle Mass Analysis by Rayleigh Light Scattering. Micelle concentration and mass are related to the refractive index of material emerging from the size exclusion column, sample absorbance, and the intensity of light scattered by the sample in the following way:

$$I_{LS} = CM_W\left(\frac{dn}{dc}\right)^2 P_\theta K_{LS} \quad (2)$$

where I_{LS} is the intensity of scattered light, C is the concentration of the particle, M_W is the molecular weight of the particle, dn/dc is the specific refractive index increment of the particle, P_θ is the form factor of the particle, and K_{LS} is an instrument (detector) constant. dn/dc describes how the refractive index of a solution varies for a given increment in concentration and is expressed as grams per milliliter (*26*). For particles with a M_W of $\leq 1 \times 10^6$, P_θ approaches 1 (*26*), giving

$$M_W = \frac{I_{LS}}{C\left(\frac{dn}{dc}\right)^2 K_{LS}} \quad (3)$$

The refractive index signal (RI) may be expressed as

$$\mathrm{RI} = K_{\mathrm{RI}} C \left(\frac{\mathrm{d}n}{\mathrm{d}c}\right) \tag{4}$$

where K_{RI} is an instrument calibration constant. Hence

$$K' = \frac{K_{\mathrm{RI}}}{K_{\mathrm{LS}} \left(\frac{\mathrm{d}n}{\mathrm{d}c}\right)} \tag{5}$$

$$M_{\mathrm{W}} = K' \frac{I_{\mathrm{LS}}}{\mathrm{RI}} \tag{6}$$

where K' is a combined constant of $(\mathrm{d}n/\mathrm{d}c)\ K_{\mathrm{LS}}/K_{\mathrm{RI}}$. For a protein containing heterogeneous carbohydrate chains, $\mathrm{d}n/\mathrm{d}c$ is not known or may not be constant. Fortunately, the UV absorbance of the sample is related to C through the relationship

$$\mathrm{uv} = K_{\mathrm{UV}} C \epsilon \tag{7}$$

where K_{UV} is an instrument constant and ϵ is the extinction coefficient (sample absorbance at 1 mg/mL with a 1 cm path length). Thus

$$M_{\mathrm{W}} = \frac{{K_{\mathrm{RI}}}^2 I_{\mathrm{LS}} \mathrm{uv}}{K_{\mathrm{LS}} K_{\mathrm{UV}} \epsilon (\mathrm{RI})^2} \tag{8}$$

Wen et al. (*26*) demonstrate that when ϵ_{P} (extinction of the carbohydrate-free polypeptide) is known at a wavelength where the extinction coefficient of a carbohydrate equals 0 (e.g., 280 nm), ϵ_{P} can be substituted for ϵ (above).

RESULTS

Dynamic Light Scattering. The hydrodynamic radius (R_{h}) of bovine serum albumin ($M_{\mathrm{W}} = 67$ kDa; 1 mg/mL) was obtained by size exclusion chromatography (using standards with R_{h} values ranging from 1.8 to 8.5 nm to calibrate the column) and by dynamic light scattering (Figure 1). The result ($R_{\mathrm{h}} = 3.48 \pm 0.12$ nm; $T = 20$ °C) is method-independent and is very similar to the expected value of 3.6 nm at 20 °C.

Detergent Micelles. The hydrodynamic radius of micelles formed from any of a number of detergents was measured by dynamic light scattering (Table 1). Figure 2 summarizes the dependence of the detergent micelle hydrodynamic radius on temperature for six detergents: NP40, Triton X-100, *n*-octyl β-glucoside, cholic acid, CHAPS, and CHAPSO. With four of the six detergents that were examined, the micellular hydrodynamic radius increases with an increase in temperature. CHAPS and CHAPSO micelle hydrodynamic radii decrease with an increase in temperature. The temperature dependence of detergent micelle R_{h} is summarized in Tables 1 and 2. With octyl glucoside, the cloud point of the detergent is 34 °C, resulting in detergent precipitation. This is rapidly reversed ($\tau \approx 2$ s) by lowering the temperature to 30 °C.

Detergent/Lipid Micelles. The goal of this study was to examine the dependence of the GLUT1 oligomeric size on the nature of the solubilizing detergent. Purified GLUT1 also contains red cell lipids [phospholipid:cholesterol:GLUT1 ratio of 1:0.3:1 by mass and 73:43:1 by molarity (*27*)]. Detergent-solubilized GLUT1 therefore contains a heterogeneous population of micelles which includes detergent micelles, detergent/lipid micelles, and detergent/lipid/GLUT1 micelles. Table 1 summarizes the hydrodynamic radii of micelles formed from lipids isolated from purified GLUT1 by organic extraction (*22*) and solubilized in various detergents. Detergent/lipid mixed micelles are significantly larger than detergent micelles but exhibit the same general temperature dependence of R_{h} that pure detergent micelles do.

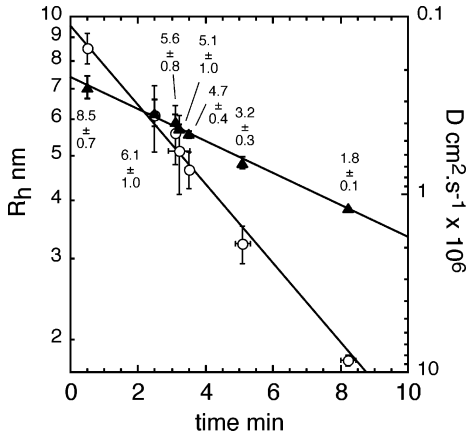

FIGURE 1: Hydrodynamic properties of water-soluble protein standards determined by dynamic light scattering and by size exclusion chromatography: (left ordinate, ○) particle Stokes radius (R_{h}) determined by DLS (nanometers, note the log scale), (right ordinate, ▲) particle diffusion coefficient (square centimeters per second; note the scale is logarithmic and inverted), and (abscissa) time of elution from the column − the void volume elution time (the latter measured using blue dextran). The standards employed are as follows (in order of elution from the column): thyroglobulin ($M_{\mathrm{r}} = 749$ kDa), ferritin ($M_{\mathrm{r}} = 421$ kDa), catalase ($M_{\mathrm{r}} = 211$ kDa), IgG ($M_{\mathrm{r}} = 154.33$ kDa), aldolase ($M_{\mathrm{r}} = 154.33$ kDa), BSA ($M_{\mathrm{r}} = 69.51$ kDa), and lysozyme ($M_{\mathrm{r}} = 13.71$ kDa). Each point represents the mean of three or more measurements at 20 °C. The numbers shown in parentheses are the R_{h} values ± the SEM of each standard as measured by DLS. The lines drawn through the points were computed by nonlinear regression assuming particle size and diffusion coefficient display an exponential dependence on elution time. The curves have the following properties: $R_{\mathrm{h}} = (9.41 \pm 0.13\ \mathrm{nm})\mathrm{e}^{-t(0.288 \pm 0.004\ \mathrm{min}^{-1})}$ ($R^2 = 0.998$) and $D = [(2.19 \pm 0.09) \times 10^{-7}\ \mathrm{cm}^2\ \mathrm{s}^{-1}]\mathrm{e}^{-t(0.207 \pm 0.006\ \mathrm{min}^{-1})}$ ($R^2 = 0.995$).

Detergent/Lipid/GLUT1 Micelles. Detergent/lipid/GLUT1 micelle hydrodynamic radii are strongly dependent on the nature of the detergent (Table 1), but in all instances, R_{h} increases with temperature (Table 1). With CHAPS- and CHAPSO-solubilized GLUT1, this behavior differs significantly from the temperature dependence of the detergent or detergent/lipid micelle R_{h} (Table 2 and Figure 2).

Rayleigh Light Scattering. Detergent/Lipid/GLUT1 micelle mass was computed by analysis of Rayleigh light scattering measurements (Figure 3). Octyl glucoside-solubilized, non-reduced GLUT1 emerges from a size exclusion column with an average R_{h} of 9.8 nm (20 °C). Measurements of micellular specific refractive index, UV absorption, and light scattering intensity permit computation of the octyl glucose/lipid/GLUT1 micellular M_{W} (400 kDa) (Table 3). When GLUT1 is purified in the presence of reductant (Figure 3B), the R_{h} and computed mass of octyl glucose/lipid/GLUT1 micelles

Table 1: Hydrodynamic Properties of Detergent/Lipid/GLUT1 Micelles

	R_h(10 °C)[a] (nm)	R_h(20 °C)[a] (nm)	molecular volume[b] (Å^3)	N(10 °C)[c]	N(20 °C)[c]	N by others[d]
			Detergent Alone			
OG	1.53 ± 0.04	1.98 ± 0.03	303.7	49	107	27
cholic acid	0.85 ± 0.07	1.00 ± 0.09	428.1	6	10	3
DDM		2.40 ± 0.07	526.8		110	98
CHAPS	1.08 ± 0.03	1.07 ± 0.03	594.8	9	9	10
CHAPSO	0.99 ± 0.06	1.46 ± 0.41	637.4	6	20	11
Triton X-100	2.35 ± 0.07	2.81 ± 0.01	750.2	72	124	140
NP40	2.07 ± 0.15	3.25 ± 0.42	802.8	47	180	100−155
digitonin		3.9 ± 0.11				
			Detergent and Lipid			
OG	2.32 ± 0.03	2.32 ± 0.02				
cholic acid	0.890 ± 0.01	1.16 ± 0.03				
DDM		2.40 ± 0.03				
CHAPS	2.36 ± 0.01	2.16 ± 0.02				
CHAPSO	2.66 ± 0.02	4.67 ± 0.41				
Triton X-100	2.83 ± 0.03	3.20 ± 0.04				
NP40	4.42 ± 0.06	5.81 ± 0.05				

	Detergent, Lipid, and GLUT1			
	R_h(10 °C)[a] (nm)	R_h(20 °C)[a] (nm)	R_h(monomer)[e]	R_h(dimer/tetramer)[e]
OG	7.53 ± 0.45	12.73 ± 0.47	4.83	7.34
cholic acid	7.34 ± 0.36	7.61 ± 0.64	3.40	5.92
DDM		9.20 ± 0.32	4.91	7.43
CHAPS	4.13 ± 0.44	4.66 ± 0.26	4.88	7.39
CHAPSO	5.19 ± 0.26	9.39 ± 0.99	5.17	7.68
Triton X-100	9.10 ± 0.41	16.47 ± 0.50	5.35	7.86
NP40	9.89 ± 0.56	14.75 ± 1.01	6.93	9.44
digitonin		4.5 ± 0.08		

[a] R_h for micelles was experimentally measured using dynamic light scattering at 10 and 20 °C. Results are shown as means ± SEM of at least three separate determinations. [b] The molecular volume (Å^3) was calculated using CS Chem 3D. [c] The number of detergent molecules present in detergent micelles was calculated using the experimentally determined R_h and the calculated molecular volumes. [d] The number of detergent molecules present in detergent micelles as reported in the literature (*29*). [e] Calculation of the theoretical R_h of micelles (detergent/lipid/GLUT1) containing one, two, or four GLUT1 proteins and an accompanying annulus of detergent and lipid. See the text for a description of the calculation.

are reduced significantly to 6.7 nm and 240 kDa, respectively (Table 2).

Both the large (Figure 3A) and smaller (Figure 3B) particles detected by RI, absorbance, and light scattering contain immuno-detectable GLUT1, [^{3}H]CCB binding capacity, and reconstitutable (CCB-inhibitable) sugar transport activity indicating that the GLUT1 present in each micellular particle is capable of ligand binding (prior to detergent solubilization) and sugar transport upon reconstitution into detergent-free lipid bilayers.

Electron Microscopy. Octyl glucoside-solubilized GLUT1 micelles were also examined by rotary shadowing transmission electron microscopy (Figure 4A,B). This procedure reveals the presence of ring-shaped particles with an average radius of 8 ± 1 nm. In the absence of GLUT1, octyl glucoside-solubilized red cell lipids form 3 nm particles as detected by negative stain EM (Figure 4C).

Freeze-fracture electron microscopy of nonreduced GLUT1 indicates the presence of integral membrane particles with an average diameter of 10 nm and a surface area of 80.1 ± 4.7 nm^2 (Figure 5A,C,E). Inclusion of a reductant during GLUT1 purification results in the generation of somewhat smaller membrane particles with a diameter of 5.5−7.2 nm and a surface area of 38.4 ± 2.5 nm^2 (Figure 5B−D). The dimensions of homology-modeled monomeric GLUT1 normal to the plane of the bilayer (*12*) indicate a molecular area of 18.2 nm^2 (Figure 5F). These simple comparisons suggest that nonreduced and reduced GLUT1 membrane particles contain 4.4 and 2.1 GLUT1 molecules, respectively. The size of integral membrane particles formed by GLUT1 reconstitution from detergents other than octyl glucoside was not investigated.

Reversibility. GLUT1 solubilization in dodecyl maltoside at 4 °C results in the time-dependent decay ($t_{0.5}$ = 2 h) of initially large particles (R_h = 8.9 nm) to smaller particles (R_h = 5 nm) upon warming to 20 °C as judged by dynamic light scattering (*13*). GLUT1 solubilization in CHAPS results in the production of small GLUT1/lipid/detergent micelles, while solubilization in octyl glucoside, Triton X-100, or cholic acid produces larger GLUT1/lipid/detergent micelles (see here and ref *13*). Most reconstitution studies performed in this laboratory have employed GLUT1 proteoliposomes produced from Triton X-100, cholic acid, or octyl glucoside-solubilized GLUT1. We were interested, therefore, in determining whether (1) the use of a detergent that normally promotes formation of small GLUT1/lipid/detergent micelles affects reconstitutable sugar transport activity upon detergent removal and (2) micelle size is irreversibly determined by the choice of the initial solubilizing detergent.

Figure 6 demonstrates that CHAPS or DDM replacement by dialysis against OG does not restore GLUT1/lipid/detergent micelle size to an R_h of 9 nm. However, CHAPS- or DDM-solubilized GLUT1 is capable of sugar transport upon reconstitution into lipid bilayers. This reconstituted transporter is restored to an R_h of 9 nm upon subsequent solubilization in OG.

DISCUSSION

This study was carried out to examine GLUT1 quaternary structure by using independent but complementary method-

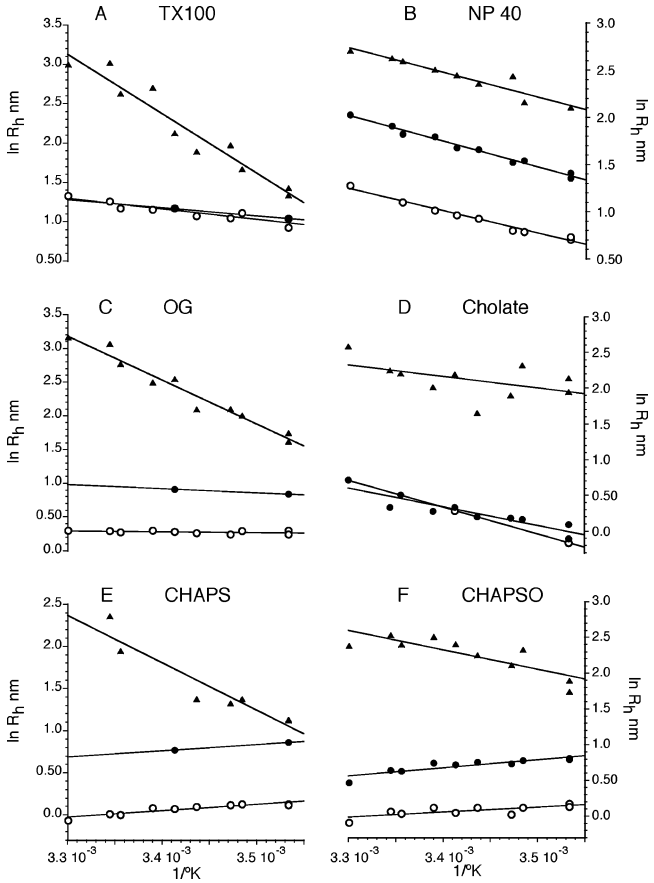

FIGURE 2: Dependence of detergent, detergent/lipid, and detergent/lipid/GLUT1 micelle hydrodynamic radius on temperature: (ordinate, panels A−F) LN micelle hydrodynamic radius (nanometers, measured by DLS) and (abscissa, panels A−F) 1/*T* (per kelvin). Lipids were extracted from purified GLUT1 proteoliposomes. GLUT1 proteoliposomes were purified from human red blood cells. The following detergents were used: (A) Triton X-100 (2%), (B) NP40 (2%), (C) octyl glucoside (60 mM), (D) sodium cholate (50 mM), (E) CHAPS (45 mM), and (F) CHAPSO (50 mM). Results are shown for detergent micelles (○), detergent/lipid micelles (●), and detergent/lipid/GLUT1 micelles (▲). Each data point is the average of at least five measurements at each temperature, and the SEM does not exceed 15% for any point. The lines drawn through the points were computed by linear regression, and constants are listed in Table 2.

ologies and to examine the influence of membrane-solubilizing detergents on GLUT1/lipid/detergent micelle hydrodynamic radii. GLUT1 forms a multimeric (probably tetrameric) complex in octyl glucoside. GLUT1 oligomeric size is decreased by reductant, and some detergents promote the reversible dissociation of GLUT1 oligomers into smaller aggregation states.

Dynamic Light Scattering Studies. DLS provides a convenient means of determining the diffusion coefficients (*D*) of large molecules (M_r > 20 kDa) and small particles (diameter < 1 μM) by measuring the rapid fluctuations in scattered light resulting from the Brownian motion or diffusion of particles in the path of incident light (*28*). The frequency of these fluctuations is directly proportional to the rate of particle diffusion which is inversely related to the size or hydrodynamic radius (R_h) of the particle [$R_h = kT/(6\pi\eta D)$].

Each detergent examined in this study presents characteristic micellular properties. For example, CHAPS and

Table 2: Constants for the Temperature Dependence of Micellular R_h Values[a]

	ΔH[b] (kcal/mol)	slope[c] ($-\Delta H/R$)	*y*-intercept[d]
	Detergent Alone		
OG	0.2	116 ± 90	0.675 ± 0.3
cholic acid	7.4	−3733	13.0
DDM			
CHAPS	−1.5	752 ± 114	−2.51 ± 0.4
CHAPSO	−1.4	699 ± 221	−2.32 ± 0.8
Triton X-100	2.7	−1340 ± 192	5.72 ± 0.7
NP40	4.7	−2362 ± 125	9.04 ± 0.4
	Detergent and Lipid		
OG	1.2	−601	2.96
cholic acid	5.2	−2600 ± 395	9.19 ± 1.3
DDM			
CHAPS	−1.5	−741	−1.76
CHAPSO	−2.2	−1124 ± 209	−3.11 ± 0.7
Triton X-100	2	−1012	4.62
NP40	5.8	−2719 ± 119	10.99 ± 0.5
	Detergent, Lipid, and GLUT1		
OG	13	−6527 ± 477	24.73 ± 1.6
cholic acid	3.2	−1595 ± 983	7.59 ± 3.4
DDM			
CHAPS	11.2	−5629 ± 885	20.97 ± 3.1
CHAPSO	5.4	−2708 ± 655	11.54 ± 2.2
Triton X-100	15	−7556 ± 716	28.07 ± 2.5
NP40	5.2	−2619 ± 274	11.38 ± 0.9

[a] This table summarizes computed linear regression constants for the temperature dependence of detergent micelle hydrodynamic radii (data shown in Figure 2). Each plot in Figure 2 is characterized by a slope. [b] ΔH is computed from the slope. [c] $\Delta H/R$. [d] Extrapolated *y*-intercept where *R* is the gas constant.

CHAPSO (related zwitterionic detergents) indicate negative standard enthalpies (R_h decreases with an increase in temperature), while the nonionic detergents Triton X-100 and NP40 display strongly positive standard enthalpies (R_h increases with an increase in temperature). The octyl glucoside micellular hydrodynamic radius appears to be independent of temperature between 10 and 30 °C. Calculation of the van der Waals volume of each detergent permits computation of the aggregation number of each detergent. These are listed in Table 1 and, for most detergents, show close agreement between theory and estimates of aggregation numbers obtained in previous studies using different techniques (*29*).

Lipid/detergent micelles formed from isolated red cell lipids and detergents are typically larger than detergent micelles alone but retain the characteristic temperature dependency of size shown by detergent micelles. Thus, while the size of lipid/CHAPS micelles at 10 °C is twice that of CHAPS micelles, $\Delta H°$ remains −1.5 kcal/mol. Lipid/NP40 micelles are approximately twice as large as NP40 micelles, but $\Delta H°$ is increased only slightly from 4.7 to 5.4 kcal/mol. Assuming a phospholipid molecular volume of ≈1000 Å^3 (*30*) and that the detergent content of lipid/detergent micelles is unchanged, we compute that the average lipid/detergent micelle contains 20−70 lipid molecules. CHAPSO and NP40 micelles appear to absorb substantially more lipid, expanding to a micellular size sufficiently great to contain several hundred lipid molecules.

The size and physical properties of GLUT1/lipid/detergent micelles are significantly different from those of detergent and lipid/detergent micelles. At 10 °C, GLUT1/lipid/detergent micelles are 2−8-fold larger than their lipid/detergent micelle counterparts.

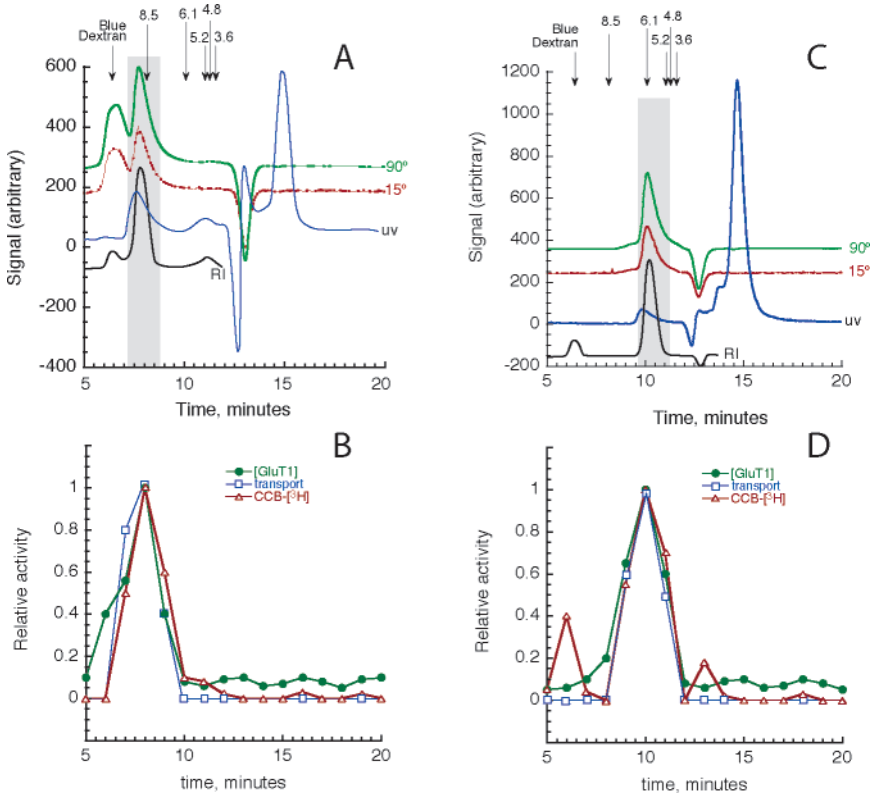

FIGURE 3: Analysis of detergent/lipid GLUT1 micelle mass by Rayleigh light scattering analysis and gel filtration. Purified nonreduced (A and B) and reduced (C and D) GLUT1 (100 μL at 1 mg/mL) were solubilized in 60 mM octyl glucoside and resolved by analytical size exclusion HPLC using a Toso Haas TSK 4000 column developed at a flow rate of 0.3 mL/min and calibrated using hydrodynamic standards obtained from Pierce. (A and C) Elution profiles detected as laser scattering at 90° (top trace), laser scattering at 15° (dashed trace), absorbance at 280 nm (third trace from top), and refractive index (bottom trace). Traces are displaced vertically to facilitate examination. The elution time of each standard (R_h in nanometers) is shown above the traces. (B and D) Elution profiles of GLUT1 detected by using C-Ab cross-reactivity (●), [^{3}H]CCB photoincorporation (△, labeling carried out prior to detergent solubilization), or reconstitutable sugar transport activity (□) following elution and detergent removal. With C-Ab binding and [^{3}H]CCB photolabeling data, each data point represents the mean of two measurements. With reconstitutable sugar transport activity data, each data point represents the average of three measurements.

Table 3: Characteristics of OG/Lipid/GLUT1 Micelles Determined by Rayleigh Light Scattering Analysis[a]

	GLUT1[b]	GLUT1[c]
dn/dc[d]	0.18 ± 0.04	0.17 ± 0.05
ϵ[e]	54188 ± 6193	54876 ± 1378
mass[f] (kDa)	406 ± 27	240 ± 12

[a] The material eluting at the times highlighted by the gray boxes in panels A and C of Figure 3 was subjected to mass analysis as described in Materials and Methods. [b] Purified in the absence of reductant. [c] Purified in the presence of reductant (20 mM DTT). [d] dn/dc is the specific refractive index increment of the particle in units of milliliters per gram. [e] ϵ is the extinction coefficient (sample absorbance at 1 mg/mL in a 1 cm path length) in units of M^{-1} cm^{-1}. [f] Mass is the computed mass of the micelles as judged by measurements of Rayleigh light scattering, refractive index, and UV absorbance at 280 nm (see Figure 3).

Assuming that the hydrodynamic radius of a detergent- or lipid-free GLUT1 monomer is identical to one-half of the membrane axis of a LacY monomer [50.28 Å/2 = 25.14 Å (*3*)] and that the R_h of a lipid/detergent micelle represents the width of a single lipid/detergent annulus surrounding the protein, it is possible to compute a hydrodynamic radius for micelles containing monomeric or dimeric/tetrameric GLUT1 (see Table 1). These arbitrary computations assume that the dimensions of individual GLUT1 subunits within multimeric GLUT1 and monomeric GLUT1 are identical. Nevertheless, the available data suggest that GLUT1 solubilized in CHAPS or CHAPSO is monomeric while GLUT1 solubilized in octyl glucoside, dodecyl maltoside, cholic acid, Triton X-100, or NP40 at 10 °C is multimeric. If GLUT1 crystallization were to require the use of monodisperse, monomeric GLUT1 micelles, the use of CHAPS or CHAPSO would be recommended.

The GLUT1/lipid/detergent micellular R_h displays a temperature dependence with all detergents (excluding NP40) significantly greater than that of lipid/detergent micelles. Moreover, R_h increases with temperature in all instances (Figure 2), indicating that $\Delta H°$ is positive. Thus, while the R_h of lipid/CHAPS or lipid/CHAPSO micelles decreases slightly with an increase in temperature, temperature-induced conformational changes in GLUT1 dominate the hydrodynamic properties of GLUT1/CHAPS(O)/lipid micelles.

Rayleigh Light Scattering. The intensity of Rayleigh or static light scattering by macromolecules in solution permits computation of molecular mass provided that the concentration of the molecule is known or can be measured coincidentally with the scattering determination (*31*, *32*). Our measurements indicate a molecular mass of GLUT1/lipid/octylglucoside micelles emerging from an analytical size exclusion column of 406 kDa (nonreduced GLUT1) and 240 kDa (reduced GLUT1). These values are very similar to determinations of the mass of nonreduced and reduced GLUT1/lipid/cholic acid micelles of 381 and 217 kDa, respectively (*18*, *33*). Assuming each GLUT1 monomer (55 kDa) is associated with 49 detergent molecules (Table 1;

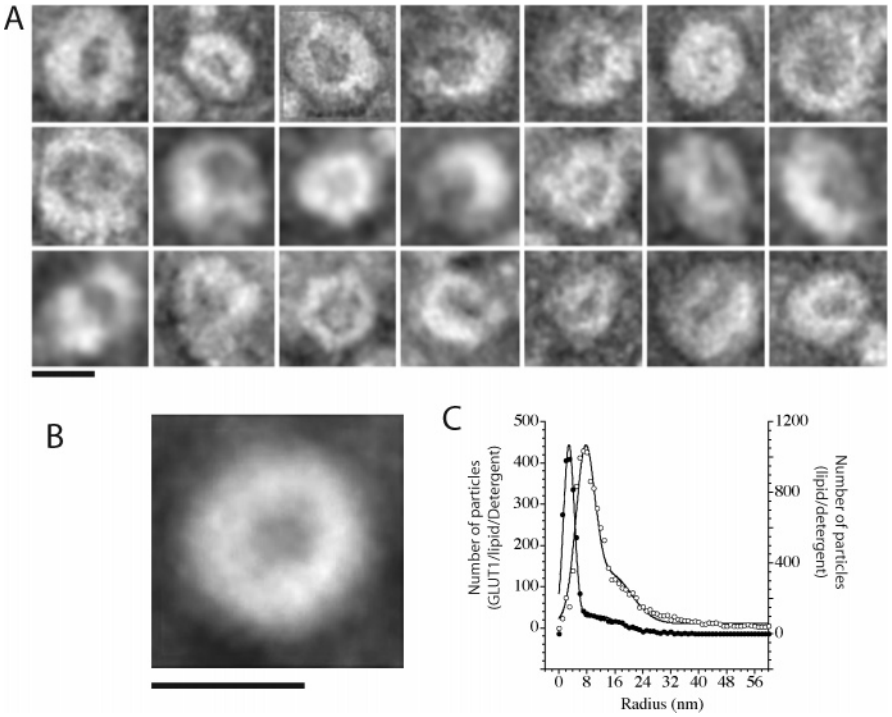

FIGURE 4: Analysis of detergent/lipid GLUT1 micelles by rotary shadow transmission electron microscopy. (A) Twenty-one panels of 60 mM octyl glucoside-solubilized, nonreduced, purified GLUT1 particles made visible by negative staining. The bar represents 10 nm. (B) Composite of 60 mM octyl glucoside-solubilized, nonreduced, purified GLUT1 particles made visible by negative staining. The bar represents 10 nm. This image represents the average of 40 particles. (C) Particle size analysis. Five micrographs of GLUT1/lipid/detergent micelles and three of lipid/detergent micelles were digitized and particle radius distributions measured using NIH Image: (ordinate) number of GLUT1/lipid/detergent (○) or lipid/detergent (●) particles detected. The curves drawn through the points were computed by nonlinear regression assuming that both GLUT1/lipid/detergent and lipid/detergent particle populations are comprised of two (large and small) particles (see Materials and Methods). The results are as follows: GLUT1/lipid/detergent, $\beta_1 = 3.1$, $\alpha_1 = 117 \pm 18$, $\mu_1 = 14.7 \pm 2.4$ nm, $\sigma_1 = 6.1 \pm 1.5$ nm, $\beta_2 = 7.1$, $\alpha_2 = 373 \pm 50$, $\mu_2 = 7.6 \pm 0.1$ nm, $\sigma_2 = 3.8 \pm 0.4$ nm, and $R = 0.986$; and lipid/detergent, $\beta_1 = 0.77$, $\alpha_1 = 1027 \pm 18$, $\mu_1 = 2.9 \pm 0.1$ nm, $\sigma_1 = 2.3 \pm 0.1$ nm, $\beta_2 = 0.77$, $\alpha_2 = 100 \pm 11$, $\mu_2 = 10.9 \pm 2.2$ nm, $\sigma_2 = 8.5 \pm 3.0$ nm, and $R = 0.986$.

the molecular weight of octyl glucoside equals 292.4 Da) and 37 phospholipids (phosphatidylcholine has an average molecular weight of 760 Da), the mass of a GLUT1/lipid/octyl glucoside micelle containing a single GLUT1 molecule would be expected to be 97.4 kDa. This suggests that the small GLUT1-containing micelles contain at least two GLUT1 proteins while the larger particle contains at least four GLUT1 proteins.

These micelles contain the majority of the GLUT1 applied to the size exclusion column as judged by the GLUT1 content assayed by an ELISA using anti-GLUT1 carboxyl-terminal IgGs. These micelles also contain all of the reconstitutable, cytochalasin B-inhibitable sugar transport activity recovered from the column and almost all of the GLUT1 protein that contains [^{3}H]CCB incorporated by photoirradiation prior to GLUT1 solubilization. Nonreduced GLUT1 contains small quantities of extremely large material as judged by material coeluting at the void volume with blue dextran. These aggregates are characterized by a low refractive index but great 90° scattering. There is a suggestion of incorporation of [^{3}H]CCB into this material prior to solubilization as judged by a leading shoulder of activity preceding the main [^{3}H]CCB peak that elutes from the column at an R_h of 9 nm.

Electron Microscopy. Octyl glucoside-solubilized, nonreduced GLUT1 is resolved by rotary shadowing transmission electron microscopy as a doughnut- or horseshoe-shaped particle with an average radius of $\approx 7.6 \pm 0.1$ nm. This is consistent with hydrodynamic radii of octyl glucoside-solubilized GLUT1 of 7.53 and 12.7 nm at 10 and 20 °C, respectively. Lipid/detergent micelles are considerably smaller (radius $= 2.9 \pm 0.1$ nm) and less structurally defined. Both GLUT1/lipid/detergent micelles and lipid/detergent micelles also contain low-abundance populations of larger particles with radii of 14.7 and 10.9 nm, respectively.

Freeze-fracture electron microscopy demonstrates that nonreduced GLUT1 forms arrays or clusters of integral membrane particles in which individual particles appear somewhat doughnut-shaped. The average radius of these particles is 4.95 nm. If an annulus of lipid and detergent were added to these particles, the radius would be increased by approximately 1.15 nm to 6.1 nm. This is smaller than the R_h of GLUT1/lipid/OG micelles as observed by dynamic light scattering (7.5 nm) but is greater than the R_h expected for a lipid/OG micelle containing only a single GLUT1 protein (4.8 nm).

FFEM studies of reduced GLUT1 reveal a somewhat smaller particle with a radius of 2.75−3.6 nm. If an annulus of lipid and detergent were added to these particles, the radius would be increased by approximately 1.15 nm to 3.9−4.75 nm. This is significantly smaller than the R_h of GLUT1/lipid/OG micelles as observed by dynamic light scattering (7.5 nm) and is smaller than the R_h expected for a lipid/OG micelle containing only a single GLUT1 protein (4.8 nm).

The reasons for these differences are unclear and suggest either that GLUT1 folding or shape is modified in the

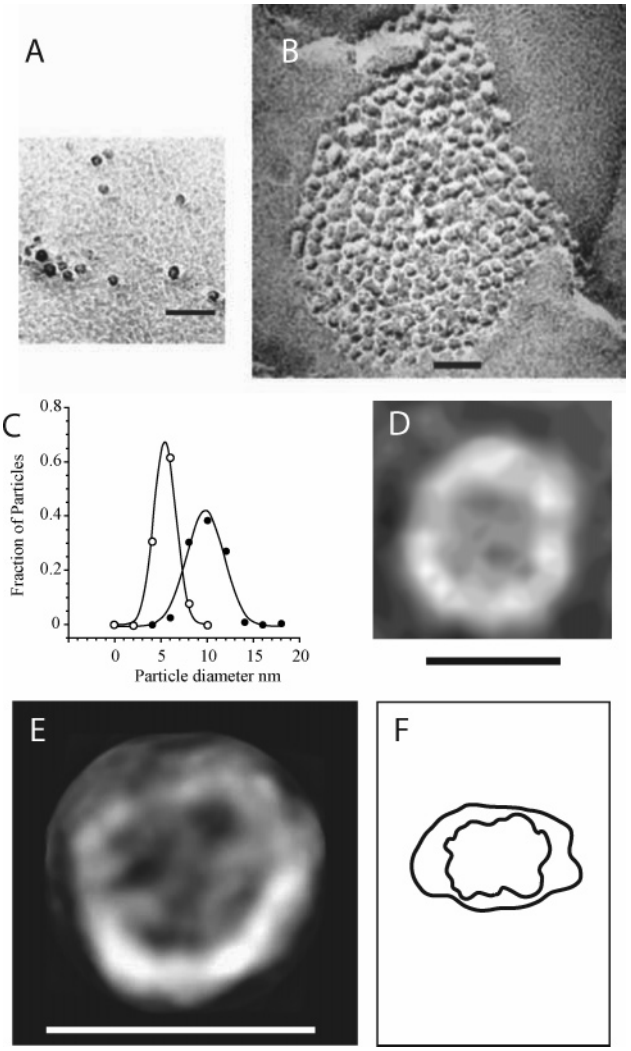

FIGURE 5: High magnification of unidirectionally shadowed freeze-fractured electron micrographs of GLUT1 proteoliposomes. (A) A cluster of P-face IMPs in reduced GLUT1 proteoliposomes. (B) A latticelike structure of P-face IMPs in nonreduced GLUT1 proteoliposomes. Bars in panels A and B represent 30 nm. (C) Particle size analysis. Freeze-fracture electron micrographs were digitized and particle radius distributions measured using NIH Image: (ordinate) fraction of the number of reduced (○) or nonreduced (●) GLUT1 proteoliposome IMPs detected. The curves drawn through the points were computed by nonlinear regression assuming that reduced and nonreduced GLUT1 proteoliposomes contain a single but unique population of IMPs (see Materials and Methods). The results are as follows: reduced GLUT1, $\beta_1 = -0.003$, $\alpha_1 = 0.67 \pm 0.01$, $\mu_1 = 5.5 \pm 0.1$ nm, $\sigma_1 = 1.7 \pm 0.1$ nm, and $R^2 = 0.999$; and nonreduced GLUT1, $\beta_1 = -0.008$, $\alpha_1 = 0.43 \pm 0.03$, $\mu_1 = 9.9 \pm 0.2$ nm, $\sigma_1 = 2.9 \pm 0.3$ nm, and $R^2 = 0.970$. (D) Composite of reduced, purified GLUT1 IMPs. The bar represents 10 nm. This image represents the average of 40 particles. (E) Composite of nonreduced, purified GLUT1 IMPs. The bar represents 10 nm. This image represents the average of 20 particles. (F) Dimensions of monomeric GLUT1 threaded through GlpT structure (*12*). The scale is identical to that of panels D and E. The irregular shapes represent the exofacial (inner outline) and cytoplasmic (outer outline) perimeters of GLUT1 in the e1 configuration (*3*, *12*).

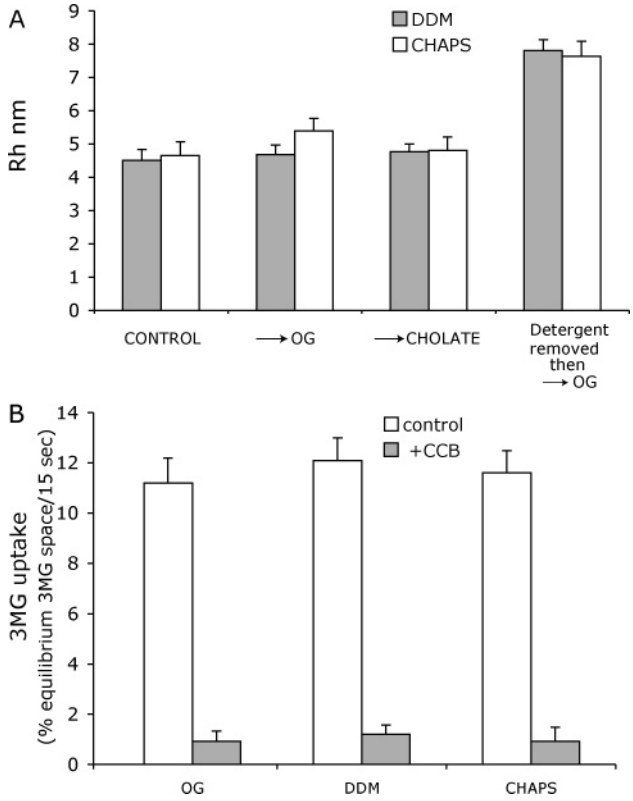

FIGURE 6: Analysis of the reversibility of action of detergents on GLUT1 structure and function. (A) Effects of detergents on GLUT1 R_h: (ordinate) GLUT1/lipid/detergent micelle R_h in nanometers and (abscissa) experimental treatment. Nonreduced GLUT1 was solubilized in dodecyl maltoside (DDM, gray bars, 40 mM) or CHAPS (white bars, 20 mM) and R_h determined by DLS. Samples were then dialyzed overnight at 4 °C against 40 mM octyl glucoside (→OG) or sodium cholate (→CHOLATE) and GLUT1 R_h values determined by DLS. Samples were also dialyzed overnight against detergent-free medium to form proteoliposomes and were subsequently resolubilized in 40 mM OG (Detergent removed then →OG) and R_h values determined by DLS. Measurements were made in triplicate and are shown as means ± SEM. (B) Effects of detergents on reconstituted GLUT1-mediated sugar transport: (ordinate) 3MG uptake by GLUT1 proteoliposomes (% 3MG equilibrium space achieved in 15 s) and (abscissa) detergent employed to solubilize GLUT1 during reconstitution into exogenous lipids [40 mM octyl glucoside (OG), 40 mM dodecyl maltoside (DDM), and 20 mM CHAPS]. Results are shown as means ± SEM of triplicate measurements. 3MG uptake (100 μM) was assessed in the presence (gray bars) and absence (white bars) of the sugar transport inhibitor CCB (20 μM).

presence of detergent or that our assumptions of lipid and detergent association with (and therefore their contribution to the hydrodynamic size of) GLUT1 micelles are greatly underestimated. Some support for this latter hypothesis may be obtained from earlier studies in which direct analyses of association of lipid and cholic acid with GLUT1 in solubilized GLUT1 proteoliposomes indicate a GLUT1:lipid:cholic acid molar composition of 1:26:50. Using the simplifying assumption of this study, we compute a GLUT1:lipid:cholic acid molar composition of 1:3:10.

Assuming that underestimation of GLUT1-associated lipid and detergent accounts for the discrepancy between FFEM and RSTEM GLUT1 particle sizes, this does not abrogate the general conclusion that GLUT1 forms a multimeric species in the cell membrane. The average molecular surface area of monomeric LacY, GlpT, or homology-modeled GLUT1 normal to the plane of the bilayer is 18.2 nm^2 (*3*, *12*, *34*; see Figure 5F). GLUT1 without DTT and GLUT1 with DTT IMP molecular surface areas are 80.1 and 38.4 nm^2, respectively, suggesting that GLUT1 without DTT is a GLUT1 tetramer while GLUT1 with DTT is a GLUT1 dimer. Earlier FFEM studies of GLUT1 proteoliposomes formed

from Triton X-100-solubilized, reduced GLUT1 indicate an IMP diameter of 6.2 nm (*35*). This size is very similar to the average diameter of reduced GLUT1 IMPs observed in our study (5.5−7.2 nm).

Reversibility. GLUT1 solubilized in CHAPS forms small GLUT1/lipid/detergent micelles (R_h = 4.4 nm) and subsequent detergent replacement by dialysis against octyl glucoside or cholic acid (detergents that normally promote larger GLUT1/lipid/detergent micelles) does not affect the micellular R_h. However, removal of CHAPS by dialysis in the presence of exogenous phosphatidylcholine results in sugar transport-competent proteoliposomes. These same proteoliposomes, when solubilized in octyl glucoside, form GLUT1/lipid/detergent micelles with an R_h of 7.8 nm. This suggests that GLUT1 does not exchange readily between micelles but can self-associate when inserted in the lipid bilayer.

This conclusion is generally supported by co-immunoprecipitation studies of epitope-tagged GLUT chimeras in which differentially tagged GLUT1 constructs expressed in and solubilized from different cell populations do not co-immunoprecipitate when mixed postsolubilization but do co-immunoprecipitate when solubilized from a single cell population cotransfected with and coexpressing both transporters (K. B. Levine and A. Carruthers, unpublished observations).

CONCLUSIONS

Hydrodynamic analysis and electron microscopy of GLUT1/lipid/detergent micelles and freeze-fracture electron microscopy of GLUT1 proteoliposomes support the hypothesis that the glucose transporter is a multimeric (probably tetrameric) complex of GLUT1 proteins.

Each GLUT1 protein present in the transporter complex is hypothesized to form a functional transport pathway (*19*). LacY and GlpT crystal structures (*3*, *11*) and the homology-based GLUT1 structure (*12*) support this hypothesis and further suggest that the transport pathway isomerizes between exofacial and endofacial states. The transport pathway consists of a symmetric, catalytic core comprising N-terminal transmembrane helices 1, 2, 4, and 5 and C-terminal transmembrane helices 7, 8, 10, and 11.

This study extends these observations by demonstrating that the glucose transporter comprises multiple (probably four) copies of GLUT1. Aquaporin and aquaglyceroporin are membrane-spanning channels that catalyze transmembrane water and glycerol fluxes (*2*, *36*). Both proteins form homo-tetrameric complexes in which each subunit functions as a single transport pathway (*37*). Other transporters that form multimeric complexes in which each subunit serves as a separate transport pathway include the red cell anion transporter, AcrB, the CaATPase, CFTR, the Na−H exchanger, the Na,KATPase, LacS, and the NSS family of Na/neurotransmitter symporters (for a review, see ref *1*). In contrast, the K channel family consists of tetramers in which one functional transport pathway is formed by four monomers (*38*). Many other transporters and channels form oligomers in which the minimum catalytic unit remains undefined (*1*). Two bacterial carrier-mediated transport systems crystallized thus far appear to be monomeric (*3*, *34*), while a third transporter, the neurotransmitter/sodium symporter bacterial homologue LeuTAa, is crystallized as a homodimer in which each subunit forms a functional transport pathway (*39*). These observations suggest that membrane transporter quaternary structure is not invariantly monomeric and that a detailed understanding of carrier function may require thorough analysis of transporter quaternary structure.

REFERENCES

1. Levine, K. B., and Carruthers, A. (2004) Regulation of carrier-mediated sugar transport by transporter quaternary structure, in *Top. Curr. Genet. 9*, 67.
2. Fu, D., Libson, A., Miercke, L. J., Weitzman, C., Nollert, P., Krucinski, J., and Stroud, R. M. (2000) Structure of a glycerol-conducting channel and the basis for its selectivity, *Science 290*, 481−486.
3. Abramson, J., Smirnova, I., Kasho, V., Verner, G., Kaback, H. R., and Iwata, S. (2003) Structure and mechanism of the lactose permease of *Escherichia coli*, *Science 301*, 610−615.
4. Kaback, H. R. (2005) Structure and mechanism of the lactose permease, *C. R. Biol. 328*, 557−567.
5. Guan, L., Hu, Y., and Kaback, H. R. (2003) Aromatic stacking in the sugar binding site of the lactose permease, *Biochemistry 42*, 1377−1382.
6. Guan, L., Weinglass, A. B., and Kaback, H. R. (2001) Helix packing in the lactose permease of *Escherichia coli*: Localization of helix VI, *J. Mol. Biol. 312*, 69−77.
7. Carruthers, A. (1991) Mechanisms for the facilitated diffusion of substrates across cell membranes, *Biochemistry 30*, 3898−3906.
8. Wright, E. M. (1993) The intestinal Na^+/glucose cotransporter, *Annu. Rev. Physiol. 55*, 575−589.
9. Joost, H. G., Bell, G. I., Best, J. D., Birnbaum, M. J., Charron, M. J., Chen, Y. T., Doege, H., James, D. E., Lodish, H. F., Moley, K. H., Moley, J. F., Mueckler, M., Rogers, S., Schurmann, A., Seino, S., and Thorens, B. (2002) Nomenclature of the GLUT/SLC2A family of sugar/polyol transport facilitators, *Am. J. Physiol. 282*, E974−E976.
10. Heard, K. S., Fidyk, N., and Carruthers, A. (2000) ATP-dependent substrate occlusion by the human erythrocyte sugar transporter, *Biochemistry 39*, 3005−3014.
11. Lemieux, M. J., Song, J., Kim, M. J., Huang, Y., Villa, A., Auer, M., Li, X. D., and Wang, D. N. (2003) Three-dimensional crystallization of the *Escherichia coli* glycerol-3-phosphate transporter: A member of the major facilitator superfamily, *Protein Sci. 12*, 2748−2756.
12. Salas-Burgos, A., Iserovich, P., Zuniga, F., Vera, J. C., and Fischbarg, J. (2004) Predicting the three-dimensional structure of the human facilitative glucose transporter glut1 by a novel evolutionary homology strategy: Insights on the molecular mechanism of substrate migration, and binding sites for glucose and inhibitory molecules, *Biophys. J. 87*, 2990−2999.
13. Cloherty, E. K., Levine, K. B., and Carruthers, A. (2001) The red blood cell glucose transporter presents multiple, nucleotide-sensitive sugar exit sites, *Biochemistry 40*, 15549−15561.
14. Hamill, S., Cloherty, E. K., and Carruthers, A. (1999) The human erythrocyte sugar transporter presents two sugar import sites, *Biochemistry 38*, 16974−16983.
15. Carruthers, A., and Helgerson, A. L. (1991) Inhibitions of sugar transport produced by ligands binding at opposite sides of the membrane. Evidence for simultaneous occupation of the carrier by maltose and cytochalasin B, *Biochemistry 30*, 3907−3915.
16. Sogin, D. C., and Hinkle, P. C. (1980) Binding of cytochalasin B to human erythrocyte glucose transport, *Biochemistry 19*, 5417−5420.
17. Gorga, F. R., and Lienhard, G. E. (1982) Changes in the intrinsic fluorescence of the human erythrocyte monosaccharide transporter upon ligand binding, *Biochemistry 21*, 1905−1908.
18. Hebert, D. N., and Carruthers, A. (1992) Glucose transporter oligomeric structure determines transporter function. Reversible redox-dependent interconversions of tetrameric and dimeric GLUT1, *J. Biol. Chem. 267*, 23829−23838.
19. Zottola, R. J., Cloherty, E. K., Coderre, P. E., Hansen, A., Hebert, D. N., and Carruthers, A. (1995) Glucose transporter function is controlled by transporter oligomeric structure. A single, intramolecular disulfide promotes GLUT1 tetramerization, *Biochemistry 34*, 9734−9747.

20. Helgerson, A. L., and Carruthers, A. (1987) Equilibrium ligand binding to the human erythrocyte sugar transporter. Evidence for two sugar-binding sites per carrier, *J. Biol. Chem. 262*, 5464−5475.
21. Levine, K. B., Cloherty, E. K., Hamill, S., and Carruthers, A. (2002) Molecular determinants of sugar transport regulation by ATP, *Biochemistry 41*, 12629−12638.
22. Bligh, E. G., and Dyer, W. J. (1959) A rapid method of total lipid extraction and purification, *Can. J. Med. Sci. 37*, 911−917.
23. van Hoek, A. N., Yang, B., Kirmiz, S., and Brown, D. (1998) Freeze-fracture analysis of plasma membranes of CHO cells stably expressing aquaporins 1−5, *J. Membr. Biol. 165*, 243−254.
24. Levine, K. B., Cloherty, E. K., Fidyk, N. J., and Carruthers, A. (1998) Structural and physiologic determinants of human erythrocyte sugar transport regulation by adenosine triphosphate, *Biochemistry 37*, 12221−12232.
25. Cloherty, E. K., Levine, K. B., Graybill, C., and Carruthers, A. (2002) Cooperative nucleotide binding to the human erythrocyte sugar transporter, *Biochemistry 41*, 12639−12651.
26. Wen, J., Arakawa, T., and Philo, J. S. (1996) Size-exclusion chromatography with on-line light-scattering, absorbance, and refractive index detectors for studying proteins and their interactions, *Anal. Biochem 240*, 155−166.
27. Carruthers, A., and Melchior, D. L. (1984) A rapid method of reconstituting human erythrocyte sugar transport proteins, *Biochemistry 23*, 2712−2718.
28. Schmitz, K. S. (1990) *An introduction to dynamic light scattering by macromolecules*. Academic Press, Inc., San Diego.
29. Helenius, A., and Simons, K. (1975) Solubilization of membranes by detergents, *Biochim. Biophys. Acta 415*, 29−79.
30. Chiu, S. W., Jakobsson, E., Mashl, R. J., and Scott, H. L. (2002) Cholesterol-Induced Modifications in Lipid Bilayers: A Simulation Study, *Biophys. J. 83*, 1842−1853.
31. Santora, L. C., Kaymakcalan, Z., Sakorafas, P., Krull, I. S., and Grant, K. (2001) Characterization of noncovalent complexes of recombinant human monoclonal antibody and antigen using cation exchange, size exclusion chromatography, and BIAcore, *Anal. Biochem. 299*, 119−129.
32. Zimmerman, S. C., Zeng, F., Reichert, D. E., and Kolotuchin, S. V. (1996) Self-assembling dendrimers, *Science 271*, 1095−1098.
33. Hebert, D. N., and Carruthers, A. (1991) Cholate-solubilized erythrocyte glucose transporters exist as a mixture of homodimers and homotetramers, *Biochemistry 30*, 4654−4658.
34. Huang, Y., Lemieux, M. J., Song, J., Auer, M., and Wang, D. N. (2003) Structure and mechanism of the glycerol-3-phosphate transporter from *Escherichia coli*, *Science 301*, 616−620.
35. Hinkle, P. C., Sogin, D. C., Wheeler, T. J., and Telford, J. N. (1979) Studies of the glucose transporter from human erythrocytes reconstituted in liposomes, in *Function and Molecular Aspects of Biomembrane Transport* (Quagliariello, E., Ed.) Elsevier/North-Holland Biomedical Press, New York, p 487.
36. Neely, J. D., Christensen, B. M., Nielsen, S., and Agre, P. (1999) Heterotetrameric composition of aquaporin-4 water channels, *Biochemistry 38*, 11156−11163.
37. King, L. S., Kozono, D., and Agre, P. (2004) From structure to disease: The evolving tale of aquaporin biology, *Nat. Rev. Mol. Cell Biol. 5*, 687−698.
38. MacKinnon, R. (2003) Potassium channels, *FEBS Lett. 555*, 62−65.
39. Yamashita, A., Singh, S. K., Kawate, T., Jin, Y., and Gouaux, E. (2005) Crystal structure of a bacterial homologue of Na^+/Cl-dependent neurotransmitter transporters, *Nature 437*, 215−223.

BI060398X